

Time-dependent magneto-transport in a driven graphene spin valve

Kai-He Ding^{1,2}, Zhen-Gang Zhu², and Jamal Berakdar²

¹*Department of Physics and Electronic Science, Changsha University of Science and Technology, Changsha, 410076, China*

²*Institut für Physik, Martin-Luther-Universität Halle-Wittenberg, 06099 Halle (Saale), Germany*

Based on the time-dependent nonequilibrium Green's function method we investigate theoretically the time and spin-dependent transport through a graphene layer upon the application of a static bias voltage to the electrodes and a time-alternating gate voltage to graphene. The electrodes are magnetic with an arbitrary mutual orientations of their magnetizations. We find features in the current that are governed by an interplay of the strength of the alternating field and the Dirac point in graphene: The influence of a weak alternating field on the zero bias conductance is strongly suppressed by the zero density of state at the Dirac point. In contrast, for a strong amplitude of the alternating field the current is dominated by several resonant peaks, in particular a marked peak appears at zero bias. This subtle competition results in a transition of the tunnel magnetoresistance from a broad peak to a sharp dip at a zero bias voltage applied to the electrodes. The dip amplitude can be manipulated by tuning the ac field frequency.

PACS numbers: 85.75.-d, 75.47.-m, 81.05.Uw

I. INTRODUCTION

The discovery of graphene, a single layer of carbon, sparked a burst of research resulting in a variety of fascinating findings¹⁻⁴. The modification of the electronic properties of graphene under various external conditions have also been explored extensively. Particularly interesting examples are the response to electromagnetic fields and the frequency dependence of the conductivity⁵⁻⁷, the photon-assisted transport⁸ and current⁹, the microwave and far-infrared response¹⁰⁻¹², as well as the plasmon spectrum¹³⁻¹⁵. In addition, new electromagnetic modes akin to graphene have been predicted^{16,17} and it was argued that graphene responds intrinsically in a non-linear manner to electromagnetic radiations and may serve thus as a natural frequency multiplier with potential applications in terahertz electronics¹⁸.

Recently, considerable attention was devoted to the spin-dependent transport in graphene and graphene-ferromagnet heterostructures, as prototypical spintronic systems¹⁹⁻²⁶. Several groups have been successful in experimentally contacting graphene to ferromagnetic electrodes²⁵ such as cobalt electrodes^{20,21} and permalloy electrodes²². This rendered possible the demonstration of spin injection into a graphene thin film by means of nonlocal magnetoresistance measurements. Further experiments evidenced a rather long spin-flip relaxation length $\approx 1\mu\text{m}$ in a single layer graphene even at room temperatures²⁰. An anomalous cusp-like feature of the magnetoresistance versus the applied bias was observed in a graphene-based spin-valve devices²³. Following these works, Ding *et al.*²⁴ studied theoretically the spin-dependent transport through the graphene spin valve device, and pointed out that the cusp-like feature at zero bias is due to a subtle interplay of the graphene peculiar nature and the conventional spin-valve properties. More recently, the effects of the external conditions such as disorder²⁷ and the magnetic impurities²⁸, on the spin-dependent transport in graphene-ferromagnet heterostruc-

tures have been addressed.

On the other hand, the spin-dependent transport under an alternating (ac) field is relatively less explored. In this work, we study theoretically the spin-dependent transport through a graphene spin-valve device with statically biased ferromagnetic leads having arbitrary spin-polarization directions in the presence of an external ac field acting on the graphene monolayer in form of a gate voltage. The employed method is based on the time dependent nonequilibrium Green's function approach, as described in Refs.29,30. It is found that the current shows a peculiar behaviour when the strength of the alternating field is varied. For a small amplitude of the ac field, the zero DOS at the Dirac point of graphene suppresses strongly the ac field effect, particularly the peak at zero bias is diminished. When the ac field strength becomes sufficiently large, the insulator-like properties of graphene at the Dirac point are less relevant and a prominent peak appears in the differential conductance at zero bias. In this case, the TMR exhibits a transition from a peak to a sharp dip at a zero bias voltage. The dip magnitude can be varied by changing the ac field frequency.

II. THEORETICAL MODEL

The spin valve device under consideration here consists of a single layer of graphene sandwiched between two ferromagnetic electrodes. The magnetization \mathbf{M}_L of the left electrode is assumed to align along the y direction, while that of the right electrode \mathbf{M}_R deviates from the y direction by a relative angle θ . A dc bias V applied to the electrodes results in a longitudinal static current in graphene. In addition, we consider a harmonic ac gate voltage $V_g(t)$ with frequency ω and strength V_{ac} being applied to the graphene sheet, i.e.

$$V_g(t) = V_{ac} \cos \omega t. \quad (1)$$

The nature of the coupling of $V_g(t)$ to the graphene sheet follows from the symmetry group analysis, e.g. as done recently in Ref. [31] in full details. Inspecting the results of Ref.³¹ we conclude that $V_g(t)$ couples to the graphene sheet through the Γ_1 representation of the point group of D_{3h} at the Dirac points of graphene. In effect, $V_g(t)$ acts on the transport as ac Fermi level. Nevertheless, as shown below, this simple coupling leads to remarkable consequences for the transport and TMR³². In the present case the Hamiltonian of this system reads thus

$$H = H_L + H_R + H_G + H_T \quad (2)$$

where

$$H_L = \sum_{\mathbf{k}, \sigma} \varepsilon_{\mathbf{k}L\sigma} c_{\mathbf{k}L\sigma}^\dagger c_{\mathbf{k}L\sigma} \quad (3)$$

$$H_R = \sum_{\mathbf{k}, \sigma} (\varepsilon_{\mathbf{k}R} - \sigma \mathbf{M}_R \cos \theta) c_{\mathbf{k}R\sigma}^\dagger c_{\mathbf{k}R\sigma} - \mathbf{M}_R \sin \theta c_{\mathbf{k}R\sigma}^\dagger c_{\mathbf{k}R\bar{\sigma}} \quad (4)$$

where $\varepsilon_{\mathbf{k}\alpha\sigma}$ is the single electron energy associated with the momentum \mathbf{k} and the spin σ in the $\alpha = L, R$ electrode, $c_{\mathbf{k}\alpha\sigma}^\dagger (c_{\mathbf{k}\alpha\sigma})$ is the usual creation (annihilation) operator for an electron with the energy $\varepsilon_{\mathbf{k}\alpha\sigma}$.

Having specified the nature of the coupling of V_g to graphene we write for the graphene Hamiltonian in the tight-binding approximation

$$H_G = \sum_{i, \sigma} \epsilon(t) (a_{i, \sigma}^\dagger a_{i, \sigma} + b_{i, \sigma}^\dagger b_{i, \sigma}) - t_g \sum_{\langle i, j \rangle, \sigma} (a_{i, \sigma}^\dagger b_{j, \sigma} + \text{H.c.}) \quad (5)$$

where $a_{i, \sigma}^\dagger (a_{i, \sigma})$ creates (annihilates) an electron with the spin σ on the position \mathbf{R}_i of the sublattice A, $b_{i, \sigma}^\dagger (b_{i, \sigma})$ creates (annihilates) an electron with the spin σ on the position \mathbf{R}_i of the sublattice B, t_g is the nearest neighbor ($\langle i, j \rangle$) hopping energy in graphene layer. Measuring the energy with respect to the Dirac point of the unperturbed graphene leads to $\epsilon(t) = V_g$.

In the momentum space Eq.(5) can be rewritten as

$$H_G = \sum_{\mathbf{q}, \sigma} [\epsilon(t) (a_{\mathbf{q}, \sigma}^\dagger a_{\mathbf{q}, \sigma} + b_{\mathbf{q}, \sigma}^\dagger b_{\mathbf{q}, \sigma}) + \phi(\mathbf{q}) a_{\mathbf{q}, \sigma}^\dagger b_{\mathbf{q}, \sigma} + \phi(\mathbf{q})^* b_{\mathbf{q}, \sigma}^\dagger a_{\mathbf{q}, \sigma}] \quad (6)$$

where $\phi(\mathbf{q}) = -t_g \sum_{i=1}^3 e^{i\mathbf{q} \cdot \delta_i}$ with $\delta_1 = \frac{a}{2}(1, \sqrt{3}, 0)$, $\delta_2 = \frac{a}{2}(1, -\sqrt{3}, 0)$, $\delta_3 = a(1, 0, 0)$ (here a is the lattice spacing). Upon diagonalizing the Hamiltonian (6) one finds $E_{\pm}(\mathbf{q}) = \pm t_g |\phi(\mathbf{q})|$, which can be linearized around the \mathbf{K} points of the Brillouin zone with the dispersion given by

$$E_{\pm}(\mathbf{q}) = \pm v_F |\mathbf{q}|, \quad (7)$$

where $v_F = 3t_g a/2$ is the Fermi velocity of electron. From Eq.(6), one infers that the ac field couples to the two Dirac cones equally as a time-dependent gate voltage. Hence, it does not induce any transitions between

the valleys. Therefore, one only need to evaluate the contributions of the single valley⁵, and then multiply the final results by a factor 2. The coupling between the electrodes and the graphene is modeled by

$$H_T = \frac{1}{\sqrt{N}} \sum_{\mathbf{k} \mathbf{q} \alpha \sigma} [T_{\mathbf{k} \alpha \mathbf{q}} c_{\mathbf{k} \alpha \sigma}^\dagger a_{\mathbf{q} \sigma} + \text{H.c.}], \quad (8)$$

where $T_{\mathbf{k} \alpha \mathbf{q}}$ is the coupling matrix between the α electrode and the graphene; N is the number of sites on the sublattice A.

Using the nonequilibrium Green's function method, the electrical current can be expressed as

$$I_\alpha(t) = -\frac{ie}{h} \int_{-\infty}^t dt_1 \int \frac{d\varepsilon}{2\pi} \text{Tr} \{ [(\mathcal{G}_a^r(t, t_1) - \mathcal{G}_a^a(t, t_1)) f_L(\varepsilon) + \mathcal{G}_a^<(t, t_1)] \Gamma_L(\varepsilon) \} e^{-i\varepsilon(t_1 - t)} \quad (9)$$

where Tr is the trace in the spin space, $f_\alpha(\varepsilon)$ is Fermi distribution function, $\mathcal{G}_a^r(t, t) = \sum_{\mathbf{q} \mathbf{q}'} G_{\mathbf{q} a, \mathbf{q}' a}^r(t, t')$ and

$\mathcal{G}_a^<(t, t') = \sum_{\mathbf{q} \mathbf{q}'} G_{\mathbf{q} a, \mathbf{q}' a}^<(t, t')$ are 2×2 matrices represent-

ing the retarded green's function and the lesser Green's function, respectively. In the calculation of Eq.(9), we assume that the dominant contributions to tunneling stem from the electrons near Fermi level, and hence assume the linewidth function to be independent of \mathbf{q} . Thus, we have

$$\Gamma_\alpha = \begin{pmatrix} \Gamma_\alpha^\uparrow & 0 \\ 0 & \Gamma_\alpha^\downarrow \end{pmatrix} \quad (10)$$

with $\Gamma_\alpha^\sigma = 2\pi \sum_{\mathbf{k}} T_{\mathbf{k} \alpha \mathbf{q}}^* T_{\mathbf{k} \alpha \mathbf{q}'} \delta(\varepsilon - \varepsilon_{\mathbf{k} \alpha \sigma})$.

To calculate $\mathcal{G}_a^{r,a}(t, t')$ in Eq.(9) we carry out the gauge transformation

$$\mathcal{G}_a^{r,a}(t, t') = \tilde{\mathcal{G}}_a^{r,a}(t, t') e^{-i \int_{t'}^t dt_1 \epsilon(t_1)} \quad (11)$$

and substitute in the equation of motion. One obtains then

$$\tilde{\mathcal{G}}_a^{r,a}(t, t') = \int \frac{d\varepsilon}{2\pi} \tilde{\mathcal{G}}_a^{r,a}(\varepsilon) [1 - \tilde{\mathcal{G}}_a^{r,a}(\varepsilon) \Sigma^{r,a}(\varepsilon)]^{-1} e^{-i\varepsilon(t - t')} \quad (12)$$

where $\tilde{\mathcal{G}}_a^{r,a}(\varepsilon) = \frac{1}{N} \sum_{\mathbf{q}} g_{\mathbf{q} a, \mathbf{q} a}^{r,a}(\varepsilon)$ and $\Sigma^{r,a} = \mp \frac{i}{2} [\Gamma_L(\varepsilon) + R \Gamma_R(\varepsilon) R^\dagger]$ with $g_{\mathbf{q} a, \mathbf{q} a}^{r,a}(\varepsilon) = \frac{\varepsilon}{(\varepsilon \pm i\eta)^2 - |\phi(\mathbf{q})|^2}$, and

$$R = \begin{pmatrix} \cos \frac{\theta}{2} & -\sin \frac{\theta}{2} \\ \sin \frac{\theta}{2} & \cos \frac{\theta}{2} \end{pmatrix}.$$

Introducing a cutoff k_c leads to

$$\tilde{\mathcal{G}}_a^r(\varepsilon) = -F_0(\varepsilon) - i\pi \rho_0(\varepsilon), \quad (13)$$

$$F_0(\varepsilon) = \frac{\varepsilon}{D^2} \ln \frac{|\varepsilon^2 - D^2|}{\varepsilon^2}, \quad \rho_0(\varepsilon) = \frac{|\varepsilon|}{D^2} \theta(D - |\varepsilon|) \quad (14)$$

with $D = v_F k_c$ denoting a high-energy cutoff of the graphene bandwidth. k_c is chosen as to guarantee the

conservation of the total number of states in the Brillouin zone after the linearization of the spectrum around the K point, this is achieved following the Debye's prescription.

The lesser Green function $\mathcal{G}_a^<(t, t')$ can be derived by applying the analytic continuation rules (cf. Ref.33) to the equation of motion of the time-ordered Green's function on a complex contour (Keldysh, Kadanoff-Baym, or another choice of contour),

$$\mathcal{G}_a^<(t, t') = \int \frac{d\varepsilon_1}{2\pi} \int \frac{d\varepsilon_2}{2\pi} \tilde{\mathcal{G}}_a^<(\varepsilon_1, \varepsilon_2) e^{-i\varepsilon_1 t + i\varepsilon_2 t'} e^{-\frac{i}{\hbar} \int_{t'}^t \varepsilon(t_1) dt_1} \quad (15)$$

where $\tilde{\mathcal{G}}_a^<(\varepsilon_1, \varepsilon_2) = \tilde{\mathcal{G}}_a^r(\varepsilon_1) \Sigma^<(\varepsilon_1, \varepsilon_2) \tilde{\mathcal{G}}_a^a(\varepsilon_2)$ with $\tilde{\mathcal{G}}_a^{r,a}(\varepsilon)$ denoting the Fourier transformation of Eq.(12), and

$$\begin{aligned} \Sigma^<(\varepsilon, \varepsilon') = & i2\pi \sum_{mn} J_m\left(\frac{V_{ac}}{\omega}\right) J_n\left(\frac{V_{ac}}{\omega}\right) \\ & \times \Gamma_L f_L(\varepsilon + m\omega) \delta[\varepsilon - \varepsilon' + (m - n)\omega] \\ & + i2\pi \sum_{mn} J_m\left(\frac{V_{ac}}{\omega}\right) J_n\left(\frac{V_{ac}}{\omega}\right) \\ & \times R \Gamma_R R^\dagger f_R(\varepsilon + m\omega) \delta[\varepsilon - \varepsilon' + (m - n)\omega] \end{aligned} \quad (16)$$

where J_m is the m th order Bessel function of the first kind. The identity $e^{i\alpha \sin(\omega t)} = \sum_{m=-\infty}^{\infty} J_m(\alpha) e^{im\omega t}$ is used in the calculation of Eq.(15).

Substituting Eqs.(11) and (15) in Eq.(9), we finally obtain the time-averaged current

$$\begin{aligned} I = & \frac{e}{\hbar} \sum_m J_m^2\left(\frac{V_{ac}}{\omega}\right) \int \frac{d\varepsilon}{2\pi} \text{Tr}\{\mathcal{G}_a^r(\varepsilon) R \Gamma_R R^\dagger \mathcal{G}_a^a(\varepsilon) \Gamma_L\} \\ & \times [f_R(\varepsilon + m\omega) - f_L(\varepsilon + m\omega)]. \end{aligned} \quad (17)$$

which is an exact response of the system without imposing any restriction on the amplitude of the external electric field V_{ac} . For a weak ac field ($V_{ac} \ll \omega$), $J_m(\frac{V_{ac}}{\omega}) \approx \frac{1}{\Gamma(m+1)} (\frac{V_{ac}}{2\omega})^m$. Thus, in this case, the contributions to the tunneling from the high sidebands is suppressed. While for the large amplitude of the ac field ($V_{ac} \gg \omega$), $J_m(\frac{V_{ac}}{\omega}) \approx \sqrt{\frac{2\omega}{\pi V_{ac}}} \cos(\frac{V_{ac}}{\omega} - \frac{m\pi}{2} - \frac{\pi}{4})$. Thus, more sidebands contribute then to the transport (we note however, that we are assuming that the external ac field is harmonic. For this reason we cannot describe with the present method the case of very short pluses in which case the harmonics associated with the pulse width become also relevant). In Eq.(17), we further set the symmetrical voltage division: $\mu_{L,R} = E_F \pm \frac{1}{2}eV$, and put $E_F = 0$ in the numerical calculations. The TMR can be obtained according to the conventional definition

$$\text{TMR} = \frac{I(0) - I(\pi)}{I(0)}, \quad (18)$$

where $I(0, \pi)$ is the time-averaged current flowing through the system in the parallel (antiparallel) configuration.

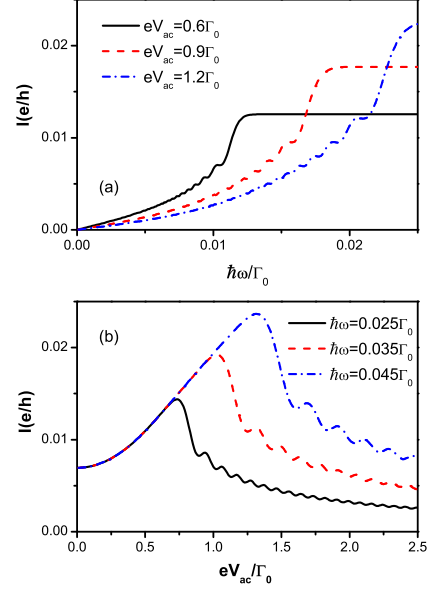


FIG. 1: (color online) The averaged current I as a function of the ac frequency for the different ac strength (a), and the ac strength for the different frequency (b) for parallel configuration of the electrodes magnetizations. The other parameters are taken as $k_B T = 0.001\Gamma_0$, $P = 0.4$, $D = 8\Gamma_0$, $eV = \Gamma_0$, where Γ_0 stands for the coupling between the scattering region and the electrodes.

III. NUMERICAL ANALYSIS

Before performing and discussing numerical calculations we shall clarify first the assumptions specific to the present theory. Adopting the wide bandwidth approximation for the graphene spin-valve system we neglect the energy dependence of the linewidth functions $\Gamma_\alpha^\sigma(\varepsilon)$. Additionally, we assume that the two electrodes are made of the same material, thus the degree of the spin polarizations of the left and the right electrodes defined by P_L and P_R can be written as $\Gamma_L^{\uparrow\downarrow} = \Gamma_R^{\uparrow\downarrow} = \Gamma_0(1 \pm P)$ where Γ_0 describes the coupling between the graphene and the electrodes in absence of an internal magnetization, and is taken as the energy scale in the following numerical calculations.

The frequency dependence of the averaged electrical current for the different ac field strength is shown in Fig.1(a). Some oscillations of the electrical current with the frequency can be seen. These oscillation peaks are asymmetric and their magnitudes depend on the weight of the different side bands (given by the Bessel functions) and is non-universal. When the frequency increases to the value $\hbar\omega \approx 0.02eV_{ac}$, the frequency dependence of the current through the graphene device acts as a pure resistance which does not vary with the frequency. Ad-

ditionally, one can easily observe that at the low frequency region, the electrical current increases when the ac strength V_{ac} grows. This result is equivalent to the one obtained in ferromagnet-insulator-ferromagnet(FM-I-FM) system³⁴. The reason for this coincidence is easy to understand: the DOS in graphene vanishes at the Dirac point. The ac field at the low frequency region stimulates the absorption and emission of photons close to the Dirac point, and thus can not break the insulator-type properties of graphene. In this case, graphene sheet can still be viewed as a tunneling barrier similar to FM-I-FM system. In the high frequency region, the photon-induced channels away from the Dirac point contribute predominantly to the transport, thus leading to the increase of the electrical current with the ac strength. The V_{ac} dependence of the electrical current for different frequencies is shown in Fig. 1(b). The current first increases with V_{ac} , and then decreases involving small oscillations when $eV_{ac} > 30\hbar\omega$. The nonmonotonic dependence of the electrical current with V_{ac} is different from FM-I-FM system. The reason is that the high sideband tunneling is dominant in the ferromagnet-graphene-ferromagnet(FM-G-FM) system, while the population probability modulation of the sidebands $J_m^2(V_{ac}/\omega)$ tends to suppress its contribution. Hence, their combinations result in the prediction that there will be a maximum in the current for some ac voltage.

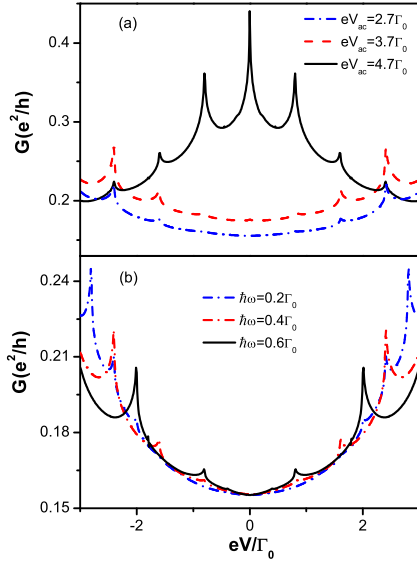


FIG. 2: (color online) The dc bias dependence of the differential conductance G for different ac strength V_{ac} at $\hbar\omega = 0.4\Gamma_0$ (a) and for different frequency ω at $eV_{ac} = 2.7\Gamma_0$ (b) for parallel configuration of the electrodes magnetizations. The other parameters are taken as those of Fig.2.

Fig.2 shows the dc bias dependence of the differential conductance $G = dI/dV$ for the different ac strength

and frequency ω in the parallel electrodes magnetizations. The differential conductance as a function of the dc voltage exhibits successive resonant peaks that correspond to a resonant tunneling through the photon-induced sidebands. It is interesting to observe that there exists a strong competition between the ac field effect and the Dirac point in graphene. For a small ac field amplitude, the zero DOS at the Dirac point of graphene suppresses strongly the ac field effect, thus diminishing the central peak (weighted by J_0^2) in the differential conductance versus the bias, as shown in Fig.2(a). When the ac field strength becomes sufficiently large, the insulator-like properties of the Dirac point of graphene are destroyed, which resembles the applied magnetic field case²⁴. If $eV = 0$, the ac field still pumps electrons through the structure behaving like an effective finite DOS. This leads to the appearance of an implicit central peak in the differential conductance at zero bias. This behavior is a marked difference to the conventional tunneling junction^{35–37}, where the central peak is preserved in the entire range of ac field strength. This characteristic features suggest that for the graphene tunneling junction, it is possible to externally manipulate the central peak induced by photon in the conductance by changing the ac field amplitude. Additionally, one can find that the sizes of the side-band peaks rise monotonously with the dc bias voltage for the small ac field amplitude, but decrease however for a sufficiently large ac field amplitude. The reason of this behaviour can be traced back to a combined effect of the ac field and the nature of graphene. For the weak ac field, the linear DOS of the graphene dominates the transport, and thus modulates the magnitude of each resonant peak. However, when the ac field becomes sufficiently strong, the population probability of the sidebands is suppressed leading to the decrease of the resonant peaks versus the bias. Fig.2(b) shows that with increasing the frequency ω of the ac field, the interval between the resonant peaks increases reflecting an increase of the distance between the photonic sidebands. The additional phenomenon is that with increasing the frequency, the each side-band conductance peak shows a slight rise because of the enhance of the side-band contribution to the tunneling by its population probability.

The dc bias dependence of the differential conductance for different temperatures T and angles θ are shown in Fig.3. With increasing the temperature, the resonant peaks in the differential conductance decrease and almost vanish at larger T . This temperature dependence of the conductance peaks is similar to that of a noninteracting, single-particle resonance in the multi-channel model. The mechanism is that at high temperatures not all electron states of the low-lying subbands are fully occupied due to the occupation of the next subbands³⁸. However, near $V = 0$, the conductance is almost independent of the temperature. This characteristic feature is different from that of the graphene system in the absence of the ac field. The zero bias conductance in the latter is sensitive to the temperature²⁴. This insensitivity here can be un-

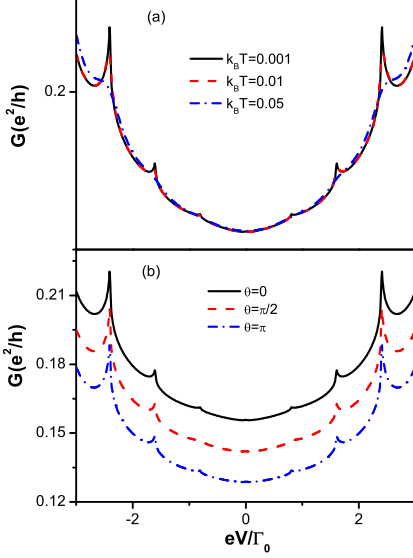


FIG. 3: (color online) The bias dependence of the differential conductance G for different temperature T at $\theta = 0$, $eV_{ac} = 2.7\Gamma_0$, $\hbar\omega = 0.4\Gamma_0$ (a) and for different angle θ at $k_B T = 0.001\Gamma_0$, $eV_{ac} = 2.7\Gamma_0$, $\hbar\omega = 0.4\Gamma_0$ (b). The other parameters are taken the same as those of Fig.2.

derstood due to a lifting of the insulator-type properties of graphene at the Dirac point in the presence of the ac field. Fig. 3(b) shows that a monotonous suppression of the differential conductance with increasing the angle θ takes place in the whole dc voltage range. This stems from the fact that when θ changes from 0 to π the number of spin-up and spin-down electrons is rearranged. Therefore the couplings for spin-up and spin-down electrons become different and the conductance decreases.

The dc bias dependence of the TMR, defined in Eq.(18), for different ac strengths V_{ac} and different frequencies ω is shown in Fig. 4. At nonzero bias voltage, the TMR has a step-like structure as a function of the bias voltage which is caused by photon-assisted effects. When increasing the ac field strength, the TMR decreases since the subbands induced by the ac field enhance the electron transport through graphene [cf. Fig. 2(a)], however they are spin independent, thus giving the same contributions to the spin-dependent transport and leading to the decrease of the TMR with the ac strength V_{ac} . However for the sufficiently large ac field strength, the TMR at the high bias voltage has a slight rise which is related to the suppress of the population probability. Remarkably, from Fig.4(a), one can see that the TMR exhibits a salient transition from a broad peak to a sharp dip at the zero bias voltage. This is due to the strong competition between the ac field effect and the Dirac point of graphene. An effective DOS developing by the large ac field strength pushes the central region

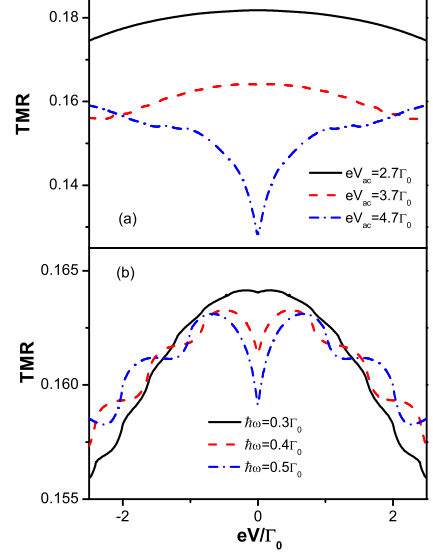


FIG. 4: (color online) The dc bias dependence of the TMR for different ac strength V_{ac} at $\hbar\omega = 0.2\Gamma_0$ (a) and for different frequency ω at $eV_{ac} = 3.2\Gamma_0$ (b). The other parameters are taken the same as those of Fig.2.

from the insulator-like to a more metal-like behaviour. This results in a strong decrease of TMR at zero bias. Additionally, one can find that with increasing the frequency, the steps in the TMR become broad due to the increase of the distance between the sidebands, as shown in Fig.4(b). In particular, with increasing the frequency, the amplitude of the dip in the TMR at zero bias increases due to the lift of the zero bias conductance by the population probability of the main sideband.

IV. SUMMARY

In conclusion, we studied theoretically the spin-dependent transport through the FM-G-FM system in the presence of an external ac field by means of the time dependent nonequilibrium Green's function approach. We obtained analytic formulas for the electrical current, and found that there exists a strong interplay between the ac field effect and the Dirac point in graphene. For a small ac field amplitude, the zero DOS at the Dirac point of graphene suppresses strongly the ac field effect, and diminishes some of the photon-induced resonant peaks in the differential conductance when varied as a function of the the bias. For a sufficiently large ac field strength, the insulator-like properties of the Dirac point of graphene are lifted which leads to the appearance of prominent resonant peaks in the differential conductance, particularly at a zero bias. In this situation, the TMR exhibits a transition from a peak to a sharp dip at the zero bias

voltage due to this subtle competition mechanism. This dip magnitude can be manipulated even by changing the ac field frequency. Therefore, it is suggested that for a graphene tunnel junction, it is possible to externally manipulate the central peak induced by photons in the conductance and the zero bias TMR by changing the ac field amplitude or frequency.

Acknowledgments

The work of K.H.D. is supported by DAAD (Germany) and by the National Natural Science Foundation of China

(Grant Nos. 10904007), the Natural Science Foundation of Hunan Province, China (Grant No. 08JJ4002), and the construct program of the key discipline in Changsha University of Science and Technology, China. J.B. and Z.G.Z. are supported by DFG, Germany.

-
- ¹ K. S. Novoselov, A. K. Geim, S. V. Morozov, D. Jiang, M. I. Katsnelson, I. V. Grigorieva, S. V. Dubonos, and A. A. Firsov, *Nature* **438**, 197 (2005).
 - ² Y. Zhang, Y. W. Tan, H. L. Stormer, and P. Kim, *Nature* **438**, 201 (2005).
 - ³ A. K. Geim and K. S. Novoselov, *Nature Materials* **6**, 183 (2007).
 - ⁴ A. H. Castro Neto, F. Guinea, N. M. R. Peres, K. S. Novoselov, A. K. Geim, *Rev. Mod. Phys.* **81**, 109 (2009).
 - ⁵ N. M. R. Peres, F. Guinea, and A. H. Castro Neto, *Phys. Rev. B* **73**, 125411(2006).
 - ⁶ L. A. Falkovsky and A. A. Varlamov, *Europ. Phys. J. B* **56**, 281 (2007).
 - ⁷ V. P. Gusynin and S. G. Sharapov, *Phys. Rev. B* **73**, 245411 (2006).
 - ⁸ B. Trauzettel, Y. M. Blanter, and A. F. Morpurgo, *Phys. Rev. B* **75**, 035305 (2007).
 - ⁹ A. S. Moskalenko, J. Berakdar, *Phys. Rev. B* **80**, 193407 (2009).
 - ¹⁰ V. P. Gusynin, S. G. Sharapov, and J. P. Carbotte, *Phys. Rev. B* **75**, 165407 (2007).
 - ¹¹ L. A. Falkovsky and S. S. Pershoguba, *Phys. Rev. B* **76**, 153410 (2007).
 - ¹² D. S. L. Abergel and V. I. Falko, *Phys. Rev. B* **75**, 155430 (2007).
 - ¹³ E. H. Hwang and S. Das Sarma, *Phys. Rev. B* **75**, 205418 (2007).
 - ¹⁴ B. Wunsch, T. Stauber, F. Sols, and F. Guinea, *New J. Phys.* **8**, 318 (2006).
 - ¹⁵ V. Apalkov, X.-F. Wang, and T. Chakraborty, *Int. J. Mod. Phys. B* **21**, 1165 (2007).
 - ¹⁶ O. Vafek, *Phys. Rev. Lett.* **97**, 266406 (2006).
 - ¹⁷ S. A. Mikhailov and K. Ziegler, *Phys. Rev. Lett.* **99**, 016803 (2007).
 - ¹⁸ S. A. Mikhailov and K. Ziegler, *J. Phys.: Condens. Matter* **20**, 384204(2008)
 - ¹⁹ E. W. Hill, A. K. Geim, K. Novoselov, F. Schedin, and P. Black, *IEEE Trans. Magn.* **42**, 2694 (2006).
 - ²⁰ N. Tombros, C. Jozsa, M. Popinciuc, H. T. Jonkman, and B. J. Van Wees, *Nature* **448**, 571 (2007).
 - ²¹ M. Ohishi, M. Shiraishi, R. Nouchi, T. Nozaki, T. Shinjo, and Y. Suzuki, *Jap. J. Appl. Phys.* **46**, L605 (2007).
 - ²² S. Cho, Yung-Fu Chen, and M. S. Fuhrer, *Appl. Phys. Lett.* **91**, 123105 (2007).
 - ²³ W. H. Wang, K. Pi, Y. Li, Y. F. Chiang, P. Wei, J. Shi, and R. K. Kawakami, *Phys. Rev. B* **77**, 020402(R) (2008).
 - ²⁴ K. H. Ding, Z.-G. Zhu, and J. Berakdar, *Phys. Rev. B* **79**, 045405 (2009); *EPL* **88**, 58001 (2009); *J. Phys.: Condensed Matter* **20**, 345228 (2008).
 - ²⁵ J. Maassen, W. Ji, H. Guo, *Nano Lett.* **11**, 151 (2011).
 - ²⁶ K. H. Ding, Z.-G. Zhu, and J. Berakdar, *EPL* **88**, 58001 (2009); *J. Phys.: Condensed Matter* **20**, 345228 (2008).
 - ²⁷ J. -C. Chen, S. -G. Cheng, S. -Q. Shen, and Q. -F. Sun, *J. Phys.: Condens. Matter* **22**, 035301 (2010)
 - ²⁸ K. H. Ding, Z. -G. Zhu, Z.-H. Zhang, and J. Berakdar, *Phys. Rev. B* **82**, 155143 (2010).
 - ²⁹ H. Haug and A. P. Jauho, *quantum kinetics in transport and optics of semiconductors* (Springer, Berlin, 1998).
 - ³⁰ J. Rammer, *Quantum Transport Theory* (Westview Press, Boulder, CO, 2004).
 - ³¹ R. Winkler, and U. Zülicke, *Phys. Rev. B* **82**, 245313 (2010).
 - ³² Other type of couplings through Γ_2 and Γ_6 representations corresponds to different physical situations and are the subject of ongoing work.
 - ³³ D. C. Langreth, in *Linear and Nonlinear Electron Transport in Solids*, edited by J. T. Devreese and V. E. Van Daren, Nato ASI, Ser. B, Vol. **17** (Plenum, New York, 1976).
 - ³⁴ Z. -G. Zhu, G. Su, Q. -R. Zheng, and B. Jin, *Phys. Rev. B* **68**, 224413 (2003)
 - ³⁵ G. Platero and R. Aguado, *Phys. Rep.* **395**, 1 (2004).
 - ³⁶ Z. -G. Zhu, G. Su, Q. -R. Zheng, and B. Jin, *Phys. Rev. B* **70**, 174403 (2004).
 - ³⁷ W. G. van der Wiel, T. H. Oosterkamp, S. De Franceschi, C. J. P. M. Harmans, and L. P. Kouwenhoven, arXiv:cond-mat/9904359.
 - ³⁸ B. J. van Wees, L. P. Kouwenhoven, E. M. M. Willems, C. J. P. M. Harmans, J. E. Mooij, H. van Houten, C. W. J. Beenakker, J. G. Williamson, C. T. Foxon, *Phys. Rev. B* **43**, 12431 (1991).